JACS
JOURNAL OF THE AMERICAN CHEMICAL SOCIETY
Article
pubs.acs.org/JACS

Complete Biosynthetic Pathway of Anditomin: Nature's Sophisticated Synthetic Route to a Complex Fungal Meroterpenoid

Yudai Matsuda, Toshiyuki Wakimoto, Takahiro Mori, Takayoshi Awakawa, and Ikuro Abe*

Graduate School of Pharmaceutical Sciences, The University of Tokyo, 7-3-1 Hongo, Bunkyo-ku, Tokyo 113-0033, Japan

Supporting Information

ABSTRACT: Anditomin and its precursors, andilesins, are fungal meroterpenoids isolated from *Aspergillus variecolor* and have unique, highly oxygenated chemical structures with a complex bridged-ring system. Previous isotope-feeding studies revealed their origins as 3,5-dimethylorsellinic acid and farnesyl pyrophosphate and suggested the possible involvement of a Diels–Alder reaction to afford the congested bicyclo[2.2.2]octane core structure of andilesins. Here we report the first identification of the biosynthetic gene cluster of anditomin and the determination of the complete biosynthetic pathway by characterizing the functions of 12 dedicated enzymes. The anditomin pathway actually does not employ a Diels–Alder reaction, but involves the nonheme iron-dependent dioxygenase AndA to synthesize the bridged-ring by an unprecedented skeletal reconstruction. Another dioxygenase, AndF, is also responsible for the structural complexification, generating the end product anditomin by an oxidative rearrangement.

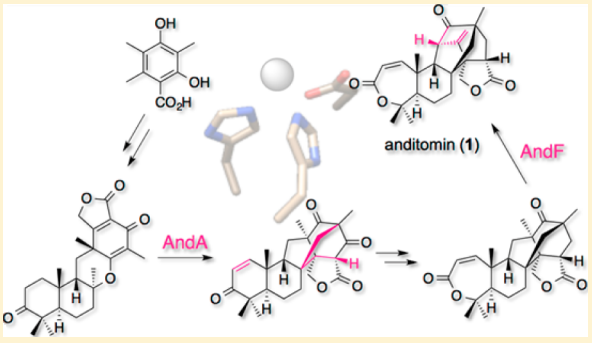

INTRODUCTION

Natural products have been attractive and rich sources for pharmaceuticals, cosmetics, fragrances, and other materials in human history. Additionally, the structural diversity and complex molecular architectures are important and intriguing characteristics of natural products, and have thus inspired many scientists to elucidate the chemistries and the genetic/molecular bases for the biosyntheses of these fascinating molecules. The frameworks of natural products are often constructed by polyketide synthases (PKSs), nonribosomal peptide synthetases (NRPSs), or terpene cyclases, and therefore these enzymes have been intensively studied to obtain insights into their reaction mechanistics that are responsible for the diversity of natural products.[1−3] In many pathways, the core scaffolds synthesized by PKSs, NRPSs, or terpene cyclases further undergo decorative reactions by tailoring enzymes, which also play a prominent role in generating the unique and congested skeletons of natural products. Despite the existence of different kinds of decorating enzymes, the complexification of natural product frameworks is frequently induced by oxygenases, including cytochrome P450 monooxygenases, nonheme iron-dependent oxygenases, and flavin adenine dinucleotide (FAD)-dependent monooxygenases. Among the fungal natural products, there have been a number of interesting reactions reported to date, including a variety of oxidative rearrangements,[4] the carbonate-forming reaction,[5] and the cyclization of a terpenoid moiety.[6] Thus, oxygenases significantly contribute to the structural diversity of natural products.

Anditomin (**1**), along with the structurally related andilesins A–C (**2**–**4**) and andibenins A–C, was isolated from *Aspergillus variecolor* around 1980,[7−10] and subsequently in 2011, emervaridione, with a similar structure to **1**, was obtained from the endophytic fungus *Emericella variecolor* (the perfect state of *A. variecolor*).[11] These compounds all possess a unique, highly oxygenated bridged-ring system (Figure 1A). Pioneering isotope-feeding studies by Simpson's and Vederas' groups revealed their natures as meroterpenoids derived from 3,5-dimethylorsellinic acid (**5**, DMOA) and farnesyl pyrophosphate (FPP), and the following biosynthetic pathway was suggested (Figure 1B).[12−16] The starter substrate **5** would be farnesylated with FPP to yield the cyclohexadienone, which then undergoes epoxidation of the terminal olefin and protonation-initiated cyclization of the farnesyl group to yield the cyclized product with a bicyclic terpenoid moiety. The triene could then undergo the intramolecular [4 + 2] cycloaddition (Diels–Alder reaction) to yield the bicyclo[2.2.2]octane system, observed in the structures of andilesins and andibenins. Further multiple oxidoreduction reactions, such as dehydrogenation, Baeyer–Villiger oxidation, and ketoreduction, would generate the structure of **2**, which could be transformed into **1** via **3** and **4**. Despite the intriguing structures, however, no genetic or molecular basis for the biosynthesis of **1** and related compounds has been reported to date. Since no evidence has been found for the existence of an enzyme that unequivocally catalyzes the Diels–Alder reaction,[17] a biosynthetic study of **1** at the enzymatic level could provide new insight into the Diels–Alderase. Furthermore, the DMOA-derived meroterpe-

Received: August 7, 2014
Published: September 12, 2014

   dx.doi.org/10.1021/ja508127q | J. Am. Chem. Soc. 2014, 136, 15326–15336

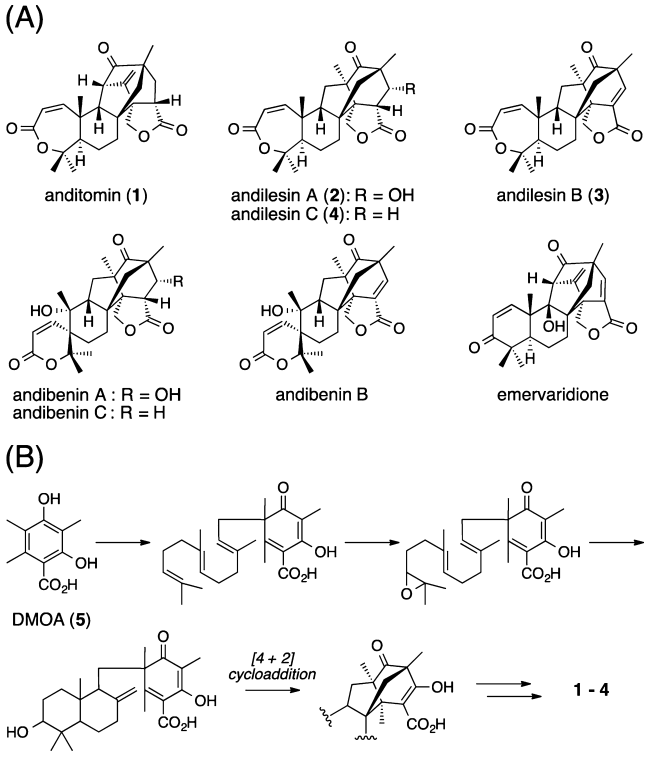

Figure 1. (A) Structures of anditomin (**1**) and related compounds. (B) Proposed early biosynthetic pathway of **1**.

noids, including **1**−**4**, comprise an especially large number of structurally diverse compounds among the fungal meroterpenoids,[18] and therefore their detailed biosynthetic mechanisms have recently been intensively studied for such molecules as austinol, terretonin, and andrastin A.[19−24] The elucidation of the molecular bases for these biosynthetically related molecules would facilitate our understanding of how fungi produce diverse compounds from simple starter substrates, and thus provide an opportunity to construct artificial metabolic pathways to afford novel scaffolds for future drug discovery.

In this study, we identified the biosynthetic gene cluster of anditomin (**1**), and analyzed the functions of each enzyme encoded by the cluster by in vivo or in vitro reconstitution of its biosynthesis. In the anditomin pathway, the nonheme iron-dependent dioxygenase AndA was found to synthesize the bicyclo[2.2.2]octane core by an unprecedented rearrangement, but not by the previously proposed Diels−Alder reaction. Another dioxygenase, AndF, also plays a key role in the structural complexification, in which andilesin C (**4**) is converted into **1** by oxidative rearrangement to complete the pathway. Finally, we have successfully established the complete biosynthetic route to **1**.

RESULTS

Discovery and Bioinformatic Analysis of the Anditomin Biosynthetic Gene Cluster. Since the genome sequences of the anditomin (**1**) producing strains were not available, we first performed the whole genome sequencing of *E. variecolor* NBRC 32302 (CMI 60316), which reportedly produces **1** and **4**.[10] By searching for a gene encoding a homologous protein to the known DMOA-producing PKSs, such as Trt4, AusA, and AdrD,[20,23,25] one gene, designated as *andM*, whose product shares more than 50% amino acid sequence identity to these enzymes and the same domain organizations, was found in the *E. variecolor* genome. Investigation of the flanking regions of the PKS gene allowed the discovery of the putative biosynthetic gene cluster of **1**, which was designated as the *and* cluster (Figure 2). The cluster encodes the typical enzymes for meroterpenoid biosyntheses, such as the prenyltransferase (AndD), the FAD-dependent epoxidase (AndE), and the terpene cyclase (AndB), and they are expected to be involved in the early biosynthetic pathway of **1**. Two nonheme iron-dependent dioxygenases (AndA and AndF), three short-chain dehydrogenases/reductases (SDRs: AndC, AndI, and AndH), an acetyltransferase (AndG), and an

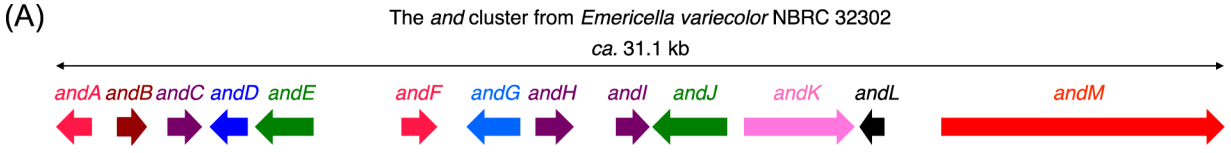

(B)

Gene	Amino acids (base pairs)	Protein homologue, origin	Similarity/identity (%)	Proposed function
andA	293 (882)	Trt7, *Aspergillus terreus*	60/36	PhyH-like dioxygenase
andB	236 (782)	AtmB, *Aspergillus flavus*	62/47	Terpene cyclase
andC	252 (940)	AdrF, *Penicillium chrysogenum*	75/59	Short chain dehydrogenase/reductase
andD	327 (984)	AdrG, *Penicillium chrysogenum*	62/49	Prenyltransferase
andE	471 (1564)	AusM, *Aspergillus nidulans*	68/51	FAD-dependent monooxygenase
andF	285 (858)	Trt7, *Aspergillus terreus*	63/43	PhyH-like dioxygenase
andG	481 (1446)	ANI_1_1240084, *Aspergillus niger*	45/26	Acetyltransferase
andH	337 (1063)	AFLA_118570, *Aspergillus flavus*	70/50	Short chain dehydrogenase/reductase
andI	290 (921)	TSTA_096040, *Talaromyces stipitatus*	68/48	Short chain dehydrogenase/reductase
andJ	633 (1902)	AusC, *Aspergillus nidulans*	68/55	FAD-dependent monooxygenase
andK	865 (2936)	MpaD/MpaE, *Penicillium brevicompactum*	67/49	Cytochrome P450 monooxygenase/hydrolase
andL	177 (688)	AFUA_3G02140, *Aspergillus fumigatus*	83/69	Hypothetical protein
andM	2430 (7499)	AdrD, *Penicillium chrysogenum*	70/54	Polyketide synthase

Figure 2. (A) Schematic representation of the *and* cluster. The direction of the arrow indicates the direction from the start to the stop codon. (B) Annotation of each protein in the *and* cluster. The deduced function of each open reading frame (ORF) and the amino acid sequence similarity/identity, as compared with the homologues found by a BLAST search at NCBI, are shown.

dx.doi.org/10.1021/ja508127q | J. Am. Chem. Soc. 2014, 136, 15326−15336

FAD-dependent monooxygenase (FMO: AndJ) are also encoded by the *and* cluster, and are presumably responsible for the tailoring reactions and engaged in the mid- and late-stages of the biosynthesis. Interestingly, no gene product from the cluster is homologous to the *O*-methyltransferases, such as Trt5, AusD, and AdrK,[19,20,23] which are present in all other reported DMOA-derived meroterpenoid gene clusters and are required for the activity of the terpene cyclases.[21,23] Alternatively, the cluster encodes a P450 monooxygenase and hydrolase fusion protein, AndK, exhibiting ∼50% identity to the MpaD/MpaE enzymes involved in the mycophenolic acid pathway.[26,27] MpaD/MpaE utilizes 5-methylorsellinic acid as its substrate to yield 5,7-dihydroxy-4-methylphthalide (DHMP), in which the P450 domain (MpaD) catalyzes the hydroxylation of the methyl group and the hydrolase domain (MpaE) forms the lactone ring. The lactonization can also occur nonenzymatically as indicated in the biosynthetic study on stipitatonic acid,[28] but the MpaE domain does have the catalytic role since the mutant lacking the hydrolase part accumulated the reaction intermediate 4,6-dihydroxy-2-(hydroxymethyl)-3-methylbenzoic acid as well as DHMP.[27] Thus, we reasoned that AndK is responsible for the similar successive reactions but accepts **5** as a substrate to afford 5,7-dihydroxy-4,6-dimethylphthalide (DHDMP). DHDMP would then undergo the transformations by the farnesyltransferase (AndD), the epoxidase (AndE), and the terpene cyclase (AndB), to produce a compound with a bicyclic terpenoid moiety similar to that shown in Figure 1B.

Early-Stage Biosynthesis of 1. To analyze the functions of the genes predicted to be responsible for the early stage biosynthesis of **1**, we undertook a heterologous expression approach in *Aspergillus oryzae* NSAR1, a quadruple auxotrophic mutant strain (*niaD*$^{-}$, *sC*$^{-}$, Δ*argB*, *adeA*$^{-}$),[29] which has been successfully applied to biosynthetic studies on fungal natural products.[21,23,24,30,31] When the PKS gene *andM* was expressed alone, the transformant produced a single product, which was not found in the control strain transformed with empty vectors (Figure 3A, lanes i and ii). As expected, ^{1}H and ^{13}C NMR and MS analyses revealed that the new product is DMOA (**5**), thus confirming that AndM is indeed the DMOA synthase. The coexpression system of *andM* and *andK* then yielded the new metabolite **6**, which eluted earlier than **5** on reverse phase HPLC chromatograms (Figure 3A, lane iii). After isolation, **6** was determined to be DHDMP (Figure 3C), demonstrating that AndK possesses the same two functions as MpaD/MpaE to produce the phthalide compound.

The further addition of the prenyltransferase gene *andD* did not result in a new product in the culture supernatant extract (Figure 3A, lane iv), but yielded the hydrophobic metabolite **7** in the mycelial extract (Figure 3B, lane ii). In the ^{1}H NMR spectrum of **7**, four allylic methyl, three olefinic methine, and several methylene signals were newly observed, and the ^{13}C NMR spectrum confirmed the presence of 25 carbons, thus indicating that a farnesyl moiety was incorporated within **6**. Two-dimensional (2D) NMR analyses then revealed the structure of **7** as a farnesylated compound at C-4 position of **6**, which was designated as farnesyl-DHDMP (Figure 3C). Unfortunately, the expected intermediate epoxyfarnesyl-DHDMP (**8**) was not isolated from the transformant with the predicted epoxidase gene *andE*, but alternatively, dihydroxyfarnesyl-DHDMP (**8′**) was detected (Figure 3A, lane v, Figure 3C). We considered **8′** to be the hydrolyzed product of the epoxide **8**, and therefore we concluded that

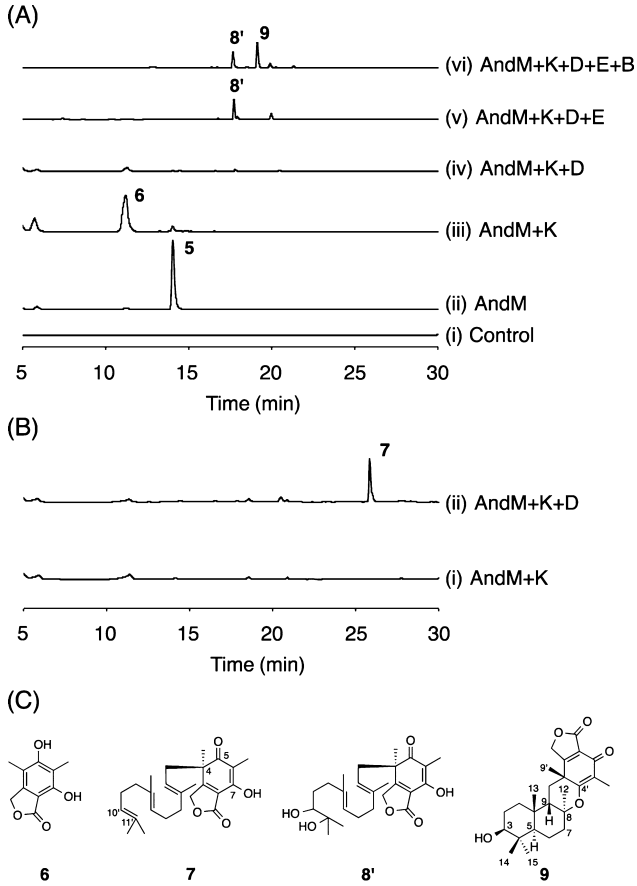

Figure 3. Reconstitution of the early stage biosynthesis of **1** in the *A. oryzae* expression system. (A) HPLC profiles of culture supernatant extracts from transformants harboring (i) only empty vectors; (ii) one gene (*andM*); (iii) two genes (up to *andK*); (iv) three genes (up to *andD*); (v) four genes (up to *andE*); (vi) five genes (up to *andB*). (B) HPLC profiles of mycelial extracts from transformants harboring (i) two genes (up to *andK*); (ii) three genes (up to *andD*). (C) Structures of compounds **6**–**9**. The chromatograms were monitored at 254 nm.

AndE is the FAD-dependent monooxygenase that forms an epoxide ring at the C-10′ and -11′ positions of **7**.

The five gene-harboring *A. oryzae* transformant with the terpene cyclase gene *andB* successfully generated the new metabolite **9** (Figure 3A, lane vi), and its molecular formula established by high resolution MS analysis ($C_{25}H_{34}O_5$) is consistent with the proposed structure. The ^{1}H NMR spectrum of **9** revealed one oxymethine signal at 3.21 ppm (dd, J = 11.9, 2.8 Hz) as well as the disappearance of all of the olefinic methine signals seen in **7** and **8′**, indicative of the opening of the epoxide ring of **8** followed by the cyclization of the farnesyl moiety. However, very surprisingly, exomethylene protons could not be observed in the spectrum, strongly suggesting that the structure with the bicyclic terpenoid moiety is incorrect. In the ^{13}C NMR spectrum, the chemical shift of C-8 in **9** was detected at 85.7 ppm, which is reminiscent of an oxygenated carbon. Additionally, two new signals at around 180 ppm appeared in the ^{13}C NMR spectrum of **9**, in place of the two carbon signals for C-5 and C-7 in **7** and **8′**. These observations indicated that the conjugated system of the phthalide-derived moiety differed from those of **7** and **8′**, due to the newly formed ether linkage between the C-4′ and C-8 positions. Further interpretation of the HMBC spectrum confirmed the planar structure of **9**, which consists of the pentacyclic core

dx.doi.org/10.1021/ja508127q | J. Am. Chem. Soc. 2014, 136, 15326−15336

Scheme 1. Complete Biosynthetic Pathway of Anditomin (1)

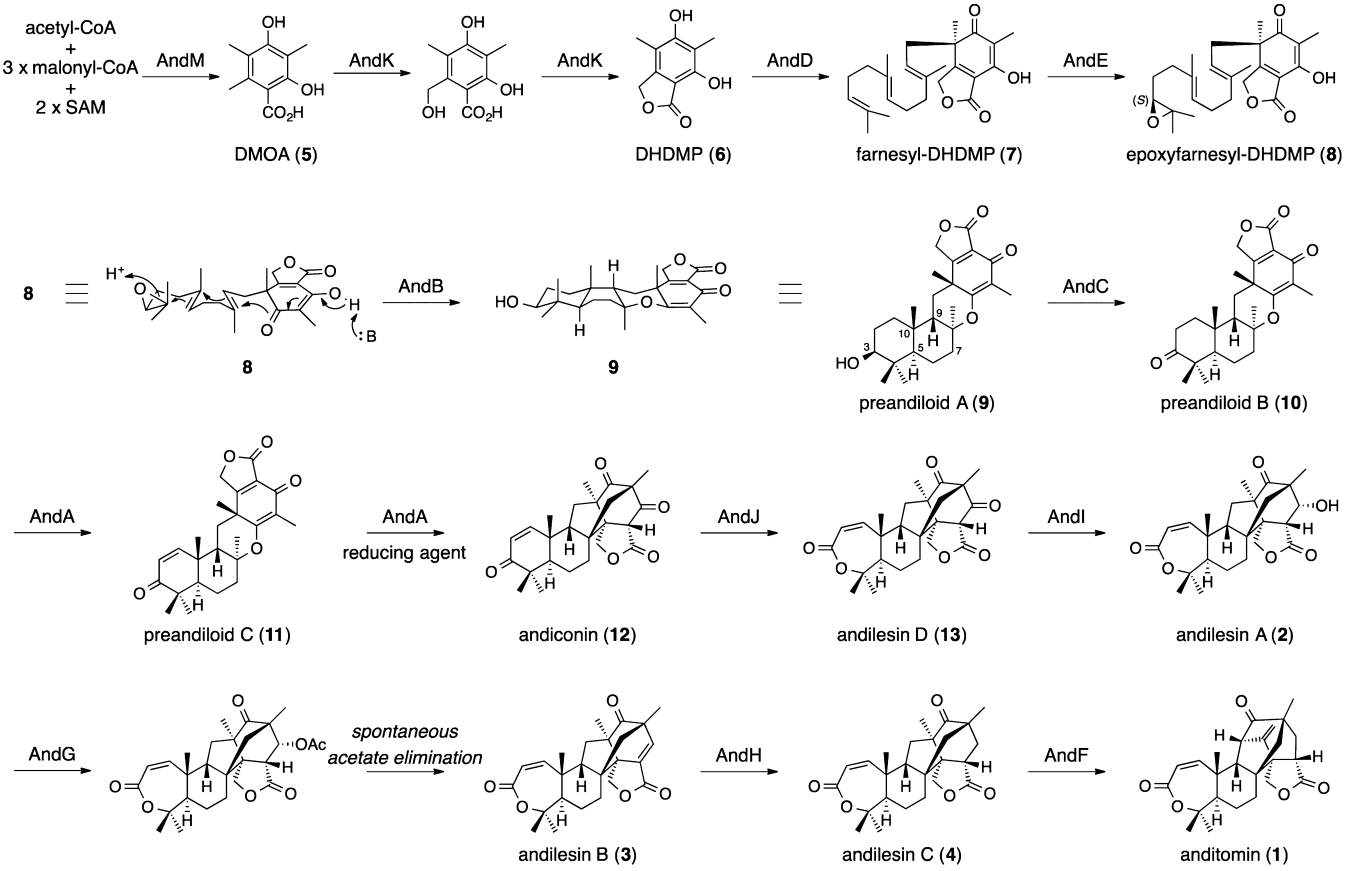

skeleton. The relative configuration of **9**, named preandiloid A, was determined by NOSEY correlations (Figure 3C, Scheme 1, Table S7): H-5 and H-3/H-7α/H-15, H-7α and H-12, H-9 and H-13/H-9′, and H-13 and H-14.

Functional Prediction of Tailoring Enzymes and Midstage Biosynthesis of 1. Although compound **9** was unexpectedly obtained, we anticipated that **9** is an intermediate of the biosynthesis of **1**, and moved onto the functional analyses of the other genes encoded by the *and* cluster. As it was difficult to predict the pathway after **9**, we performed feeding experiments of **9** (30 mg/L) to *A. oryzae* transformants harboring different combinations of the tailoring enzymes. At this point, the possible involvement of AndG, a predicted acetyltransferase, was ruled out since no acetyl group was present in the structures of **1**−**4**, which left six genes (*andA*, *andC*, *andF*, *andH*, *andI*, and *andJ*) to be analyzed. After the construction of the transformant with these six genes, it was cultivated in the presence of **9**. As a result, the strain converted **9** into the single new product **2** with *m*/*z* 429 $[M + H]^+$ (Figure 4A, lane viii), but the molecular weight of **2** was different from that of **1**. Actually, the new metabolite **2** was later found to be identical to andilesin A.

To obtain further insight into the function of each introduced gene, five gene-expression systems lacking one of the six genes were separately prepared and incubated with **9**. The two transformants without *andF* or *andH* also produced **2** (Figure 4A, lanes iv and v), indicating that AndF and AndH are not involved in the formation of **2**. In the *andC*-lacking strain, **9** remained unconverted (Figure 4A, lane iii), and thus AndC appears to utilize **9** as its substrate. Since AndC shares ∼60% sequence identity with Trt9 and AdrF, which are responsible for the oxidation of the secondary alcohol at the C-3 position in the terretonin and andrastin A pathways, respectively,[23,32] we reasoned that AndC is a dehydrogenase that oxidizes the C-3 hydroxyl group of **9** into a ketone functionality. When the nonheme iron-dependent dioxygenase gene *andA* was absent, compound **10** with similar UV absorption to that of **9** and with *m*/*z* 413 $[M + H]^+$ was obtained (Figure 4A, lane ii), and therefore **10** appears to be an oxidized product of **9** synthesized by the dehydrogenase AndC.

Product **12** from the *andJ*-lacking strain possesses *m*/*z* 411 $[M + H]^+$ and a quite different UV spectrum from those of **9** and **10** (Figure 4A, lane vii), suggesting that **12** is the oxidized product of **10** by the nonheme iron-dependent dioxygenase AndA, and that a drastic structural rearrangement occurred during the formation of **12** to generate the scaffold of andilesins. On the other hand, since AndJ is homologous to AusC (55% identity), which is a Baeyer−Villiger monooxygenase involved in austinol biosynthesis,[24] AndJ would also be responsible for the Baeyer−Villiger oxidation to generate a seven-membered lactone ring from **12**. The AndJ-product is observed in the strain not harboring *andI*, as its metabolite **13** had a 16 Da larger molecular weight than that of **12** and a similar UV spectrum (Figure 4A, lane vi). Considering that *andI* encodes a predicted SDR and that the difference in the molecular weights between **13** and **2** is 2 Da, AndI appears to reduce **13** into **2**, which is likely to be andilesin A.

To confirm the predicted pathway leading to **2** and to isolate and characterize each metabolite, we further transformed the *A. oryzae* strain synthesizing **9** with the plasmids containing the aforementioned genes. Introducing the dehydrogenase gene *andC* resulted in the appearance of **10**, as expected (Figure 4B,

dx.doi.org/10.1021/ja508127q | J. Am. Chem. Soc. 2014, 136, 15326−15336

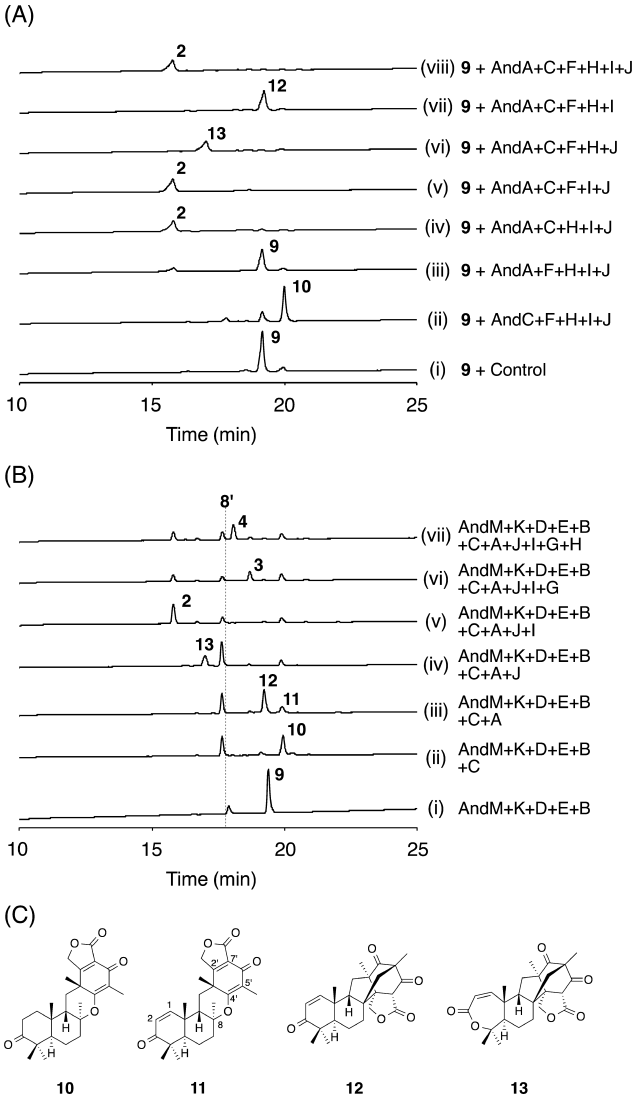

Figure 4. Functional analyses of the tailoring enzymes. (A) HPLC profiles of culture supernatant extracts from *A. oryzae* transformants incubated with **9**. Transformants (i) with only empty vectors; (ii) lacking *andA*; (iii) lacking *andC*; (iv) lacking *andF*; (v) lacking *andH*; (vi) lacking *andI*; (vii) lacking *andJ*; (viii) with *andA, C, F, H, I,* and *J*. (B) HPLC profiles of culture supernatant extracts from transformants harboring (i) five genes (up to *andB*); (ii) six genes (up to *andC*); (iii) seven genes (up to *andA*); (iv) eight genes (up to *andJ*); (v) nine genes (up to *andI*); (vi) ten genes (up to *andG*); (vii) 11 genes (up to *andH*). (C) Structures of compounds **10**–**13**. The chromatograms were monitored at 210 nm.

lane ii), and enabled the isolation and structural determination of **10**, which is indeed the ketone form of **9**, designated as preandiloid B (Figure 4C). With the addition of the nonheme iron-dependent dioxygenase *andA*, the transformant yielded not only **12** but also the minor metabolite **11** (Figure 4B, lane iii). Compound **11**, designated as preandiloid C, was found to be the dehydrogenated form of **10** with a $\Delta^{1,2}$-conjugated double bond (Figure 4C). On the other hand, the NMR spectra of **12** were very different from those of **11**, although both **11** and **12** have the same molecular formula ($C_{25}H_{30}O_5$). In the ^{1}H NMR spectrum of **12**, one singlet methine signal appeared at 3.68 ppm, and one methyl signal disappeared. Furthermore, in the ^{13}C NMR spectrum, the low magnetic field signals derived from C-8, C-2′, C-4′, C-5′, C-6′, and C-7′ of **11** all disappeared, and alternatively two signals around 200 ppm appeared, suggesting the drastic structural reconstruction to synthesize **12** in the enzymatic transformation. Further 2D NMR spectral analyses facilitated the determination of the molecular structure of **12**, which has the same bicyclo[2.2.2]octane system as the andilesins, and we named **12** andiconin (Figure 4C). The eight gene-expression system with the FAD-dependent Baeyer–Villiger monooxygenase gene *andJ* then yielded **13** as its specific metabolite (Figure 4B, lane iv), and **13**, named andilesin D, was identified as the oxidized product of **12** by Baeyer–Villiger oxidation (Figure 4C). As expected, andilesin A (**2**) was successfully obtained by further introducing *andI* (Figure 4B, lane v), establishing the biosynthetic pathway up to **2**.

In Vitro Analysis of AndA. As the reconstitution study in *A. oryzae* indicated that the nonheme iron-dependent dioxygenase AndA transforms **10** into **11** and **12**, we performed in vitro assays using recombinant AndA heterologously expressed in *Escherichia coli*. Since AndA shares sequence similarity with the members of the phytanoyl-CoA dioxygenase (PhyH) superfamily, which require Fe(II) and α-ketoglutarate (α-KG) for their activity, AndA was incubated with $FeSO_4$, α-KG, substrate **10**, and ascorbate to maintain iron in the ferrous state. The enzyme reaction generated **12** as its product (Figure 5, lane vi), and **11** was also utilized as the substrate to yield **12**

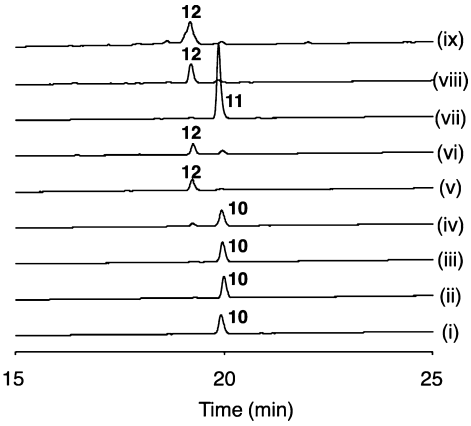

Figure 5. HPLC profiles of the products of in vitro enzymatic reactions of AndA with (i–vi) **10** or (vii, viii) **11**: (i) without AndA; (ii) without α-KG; (iii) without ascorbate; (iv) with EDTA; (v) without exogenous Fe(II); (vi) complete reaction with **10**; (vii) without AndA; (viii) complete reaction with **11**; (ix) authentic standard of **12**. The chromatograms were monitored at 210 nm.

(Figure 5, lane viii). The production of **12** was confirmed by comparing the HPLC retention time and the MS and MS^2 spectra with those of authentic **12** (Figure 5, lane ix and Figure S2). Thus, it was demonstrated that AndA is solely responsible for the intriguing structural rearrangement to generate the bicyclo[2.2.2]octane core as well as the dehydrogenation of **10** leading to the enone **11**. The enzymatic reaction proceeded in the absence of exogenous iron, probably due to residual enzyme-bound ferrous ions, but the reaction was abolished by either the presence of 1 mM EDTA or the absence of α-KG (Figure 5, lanes ii, iv, and v), indicating that AndA indeed requires Fe(II) and α-KG for the catalytic activity. Interestingly, the reaction was also almost completely abolished in the absence of ascorbate (Figure 5, lane iii). A similar phenomenon was observed in the reaction of the endoperoxide-forming

dx.doi.org/10.1021/ja508127q | J. Am. Chem. Soc. 2014, 136, 15326–15336

enzyme FtmF/FtmOX1, involved in verruculogen biosynthesis, in which ascorbate is predicted to be required for the reduction of the product radical generated by the enzyme to complete the reaction.[33,34] Considering the similar reduction by ascorbate, the transformation from **11** to **12** is not an oxidation, but an isomerization reaction.

Late-Stage Biosynthesis of 1. Given that **2**, but not **1**, was obtained in the absence of *andG* in the feeding experiment of **9**, and *andF* and *andH* were not involved in the biosynthesis of **2**, we now hypothesized that *andG* is actually engaged in the biosynthesis of **1** and that AndG accepts **2** as its substrate. AndG shares sequence similarity with the *O*-acetyltransferases, and the C-6′ hydroxyl group is the only position that can be acetylated in the structure of **2**. Therefore, we reasoned that AndG is an acetyltransferase that attaches an acetyl group to the alcohol. As no such metabolite has been isolated, and **2** is predicted to be the direct precursor of **3**, the acetylated compound could then undergo the spontaneous elimination of acetate to form the unsaturated bond of **3**.

To investigate this hypothesis, *andG* was introduced into the *A. oryzae* transformant that produces **2**, and **3** was successfully generated in an *andG*-dependent manner (Figure 4B, lane vi). To obtain deeper insight into the AndG-catalyzed reaction, in vitro assays with recombinant AndG heterologously expressed in *E. coli* were performed. Only in the presence of the enzyme and acetyl coenzyme A, the reaction proceeded to yield **3**, which was confirmed by the comparison to the authentic sample (Figure 6A, Figure S3). Additionally, the acetylation of **2** by acetic anhydride and pyridine also provided **3** (Figure 6B). Taken together, the reaction product from AndG is acetylandilesin A, which is spontaneously converted into **3** by the elimination of acetate.

The biosynthesis of **3** by AndG now led us to propose the roles of *andF* and *andH* in the anditomin pathway: the double bond of **3** would be reduced to **4** by the SDR, AndH, and this would be followed by the oxidative rearrangement catalyzed by another nonheme iron-dependent dioxygenase, AndF, to yield the end product **1**. When the 11 gene-expressing transformant with *andH* was constructed, it produced **4** as its metabolite as expected (Figure 4B, lane vii), confirming the function of AndH as the C-6′ enoylreductase of **3**.

As our attempt to construct the 12 gene-expression system with *andF* was unsuccessful, possibly due to the introduction of too many genes, we decided to characterize the function of AndF by biochemical assays with the purified recombinant enzyme from *E. coli* heterologous expression. Like AndA, AndF is predicted to be an Fe(II) and α-KG-dependent dioxygenase, and thus an in vitro assay with substrate **4** was performed in a similar manner to that described above for AndA. The complete reaction transformed **4** into **1**, which was confirmed by comparison with the authentic **1** isolated from *E. variecolor* (Figure 7, lanes vi and vii and Figure S4). AndF exhibited the same dependence as AndA on ferrous ion, EDTA, α-KG, and ascorbate (Figure 7, lanes ii–v), demonstrating that AndF requires Fe(II) and α-KG and is responsible for the very last step of the anditomin biosynthesis.

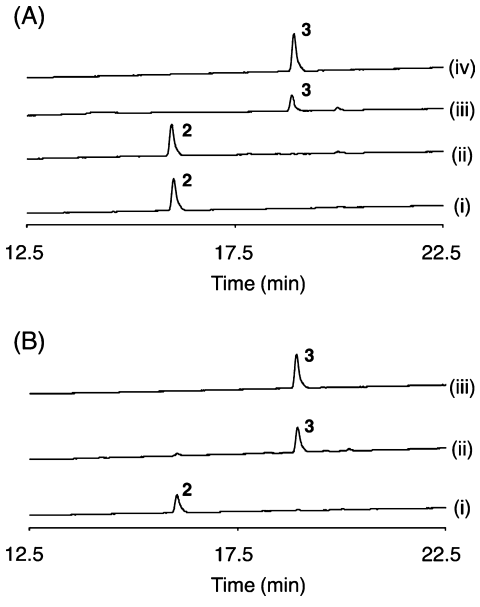

Figure 6. (A) HPLC profiles of the products of in vitro enzymatic reactions of AndG with **2**: (i) without AndG; (ii) without acetyl coenzyme A; (iii) complete reaction; (iv) authentic standard of **3**. (B) HPLC profiles of the products of acetylation of **2** with acetic anhydride and pyridine: (i) before the reaction; (ii) after the reaction; (iii) authentic standard of **3**. The chromatograms were monitored at 210 nm.

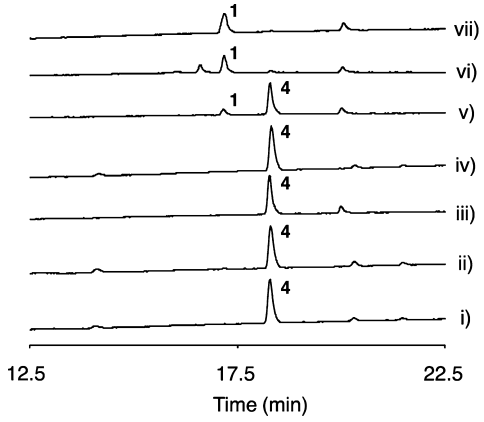

Figure 7. HPLC profiles of the products of in vitro enzymatic reactions of AndF with **4**: (i) without AndF; (ii) without α-KG; (iii) without ascorbate; (iv) with EDTA; (v) without exogenous Fe(II); (vi) complete reaction; (vii) authentic standard of **1**. The chromatograms were monitored at 210 nm.

DISCUSSION

In this study, we identified the biosynthetic gene cluster for anditomin (**1**) and characterized all of the dedicated enzymes in the anditomin pathway by in vivo or in vitro reconstitution of its biosynthesis. On the basis of our results, the complete biosynthetic pathway leading to **1** from **5** has now been fully deduced (Scheme 1). In the other reported DMOA-derived meroterpenoid pathways, such as those for terretonin, austinol, and andrastin A, DMOA is directly farnesylated by the prenyltransferase, and this is followed by the methyl ester-forming reaction by the methyltransferase.[21,23] In contrast to these pathways, anditomin biosynthesis involves the P450 monooxygenase/hydrolase, the bifunctional lactone-forming enzyme AndK, which converts **5** into the phthalide derivative **6**, and the farnesylation of **6**. Since DMOA-derived meroterpenoids comprise an especially diverse group among the fungal meroterpenoids,[18] the discovery of AndK is

dx.doi.org/10.1021/ja508127q | J. Am. Chem. Soc. 2014, 136, 15326–15336

Scheme 2. Proposed Reaction Mechanisms for the Transformations Catalyzed by (A) AndA and (B) AndF

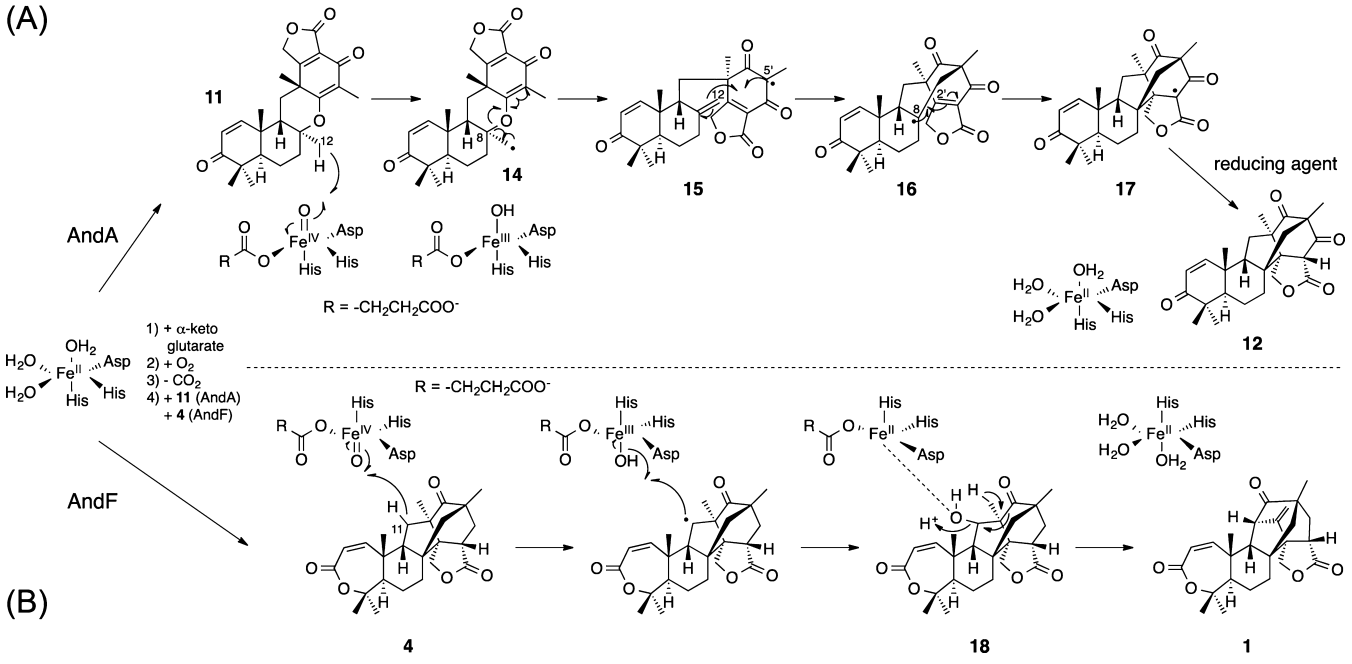

important to understand how fungi modified the pathway to use DMOA as the starter substrate.

Preandiloid A (**9**), the reaction product of the terpene cyclase AndB, consists of a pentacyclic core structure in contrast to the initial prediction, and therefore the previously proposed Diels–Alder reaction does not actually occur in the pathway. Interestingly, according to the BLAST search with AndB as a query, AndB is most homologous to AtmB (47% identity), which is involved in the biosynthesis of the indole diterpenoid aflatrem.[35] However, it exhibits relatively low sequence identity (~30% identity) to other terpene cyclases, such as Trt1, AusL, and AdrI, which are responsible for the DMOA-derived meroterpenoid pathways.[21,23] The absolute configurations of the terpenoid moiety of **9** were deduced to be 3*S*, 5*R*, 8*S*, 9*S*, 10*S*, in accordance with those of andilesin A,[8] while those of the intermediates in the terretonin, austinol, and andrastin A pathways are 3*R*, 5*S*, 8*S*, 9*S*, 10*R*. This observation provides important insight into the cyclization reactions in which the stereochemistry is strictly controlled by the enzymes. First, the absolute configurations of the substrate epoxides are different in the two pathways: the epoxyfarnesyl-DHDMP (**8**), the substrate of AndB, is an (*S*)-epoxide, while those of Trt1, AusL, and AdrI are (*R*)-epoxides. Second, the cyclization by AndB apparently proceeds with the epoxyfarnesyl moiety folded in the chair-boat conformation to generate the 3β-hydroxy functionality of **9** (Scheme 1), whereas the other three enzymes seem to adopt the chair–chair conformation of the epoxyfarnesyl-DMOA methylester to produce 3α-hydroxy scaffolds (Figure S7). Given these significant differences between the reactions by the two types of terpene cyclases, it seems reasonable that the amino acid sequence of AndB is not very homologous to those of the other terpene cyclases involved in DMOA-derived meroterpenoid biosyntheses. Finally, it is noteworthy that tropolactone D, another DMOA-derived molecule isolated from marine-derived *Aspergillus* sp., possesses a similar structure to those of **9**–**11** with 5*R*, 8*S*, 9*S*, 10*S* configurations.[36] The stereochemistry of the methyl group at C-3′ (C-12 of tropolactone D), however, is opposite between **9**–**11** and tropolactone D. As this position is the site for the attachment of the farnesyl moiety by the prenyltransferases, a farnesyltransferase with different stereoselectivity and a similar terpene cyclase to AndB may be involved in the biosynthesis of tropolactone D (Figure S8).

One of the most intriguing points in the anditomin pathway is the construction of the bicyclo[2.2.2]octane system by the multifunctional nonheme iron-dependent dioxygenase, AndA. AndA maintains a conserved 2-His-1-carboxylate iron-binding facial triad (H135, D137, H213) (Figure S9),[37] and the iron at this site would play a key role in the enzyme-catalyzed oxygenation. The detailed reaction mechanism of the rearrangement from **11** to **12** can be predicted as follows (Scheme 2A, Figure S5). The initial binding of α-KG and molecular oxygen would lead to the oxidative decarboxylation of α-KG, yielding the active Fe(IV)–oxo species. This species would abstract the hydrogen atom at the C-12 methyl group to generate the radical species **14**. The C–O bond at C-8 would then be cleaved to produce **15**, in which the radical is stabilized by delocalization. Since the tertiary radical at C-5′ is flanked by two ketone groups, it would serve as an electrophilic radical that can react with the electron-rich olefin at C-12. The resulting species **16** has a nucleophilic radical at C-8, which would then react with the electron-deficient olefin at C-2′ to yield the product radical **17**. **17**, as well as the ferric ion in the active site of the enzyme, would be reduced by ascorbate to finalize the reaction, as previously observed in the verruculogen synthase FtmF/FtmOx which is the endoperoxide bond-forming dioxygenase from *Aspergillus fumigatus*.[33,34]

Interestingly, the insuetolides isolated from *Aspergillus insuetus* have very similar structures to those of the andilesins, but contain one additional oxygen atom between C-8 and C-2′ of the andilesins (Figure S6A).[38] Considering the structural resemblance between insuetolides and andilesins, they should share similar biosynthetic processes. As it is unlikely that the oxygen atom is inserted after the formation of **12** in the insuetolides pathway, we propose that the insuetolides scaffold is generated via a similar structural reconstruction to that seen

dx.doi.org/10.1021/ja508127q | J. Am. Chem. Soc. 2014, 136, 15326–15336

in the AndA-catalyzed reaction. After the formation of **16**, if the oxygen rebound occurs, then a molecule with a C-8 hydroxyl group would be obtained. Since C-2′ of the product appears to be electrophilic, the alcohol group would spontaneously attack this position to provide the insuetolide scaffold (Figure S6B). This plausible biosynthetic mechanism of insuetolides supports the existence of **16** in the reaction with AndA and the proposed mechanism shown in Scheme 2A.

AndF, the other nonheme iron-dependent dioxygenase in the late anditomin pathway, also plays an important role in the construction of the highly congested molecular skeleton of **1**. Since AndF, like AndA, is an Fe(II)/α-KG-dependent dioxygenase, the AndF-mediated reaction should also be initiated by the abstraction of a hydrogen atom. On the basis of the previous proposal in which a C-11 cation is initially generated,[18] we propose the following mechanism for the oxidative rearrangement (Scheme 2B). The active Fe(IV)−oxo species would hydroxylate **4** at C-11, forming the Fe(II)-binding hydroxylated intermediate **18**. Elimination of the hydroxyl group as a water molecule followed by carbon skeletal rearrangement of the resulting carbocationic intermediate and deprotonation from C-9′ would yield **1**. However, as the proposed mechanism does not require an exogenous reducing agent, the reason for the requirement of ascorbate in the reaction is still elusive. The ascorbate may be used to maintain the oxidation state of AndF itself.

The acetyltransferase-mediated desaturation for the conversion of **2** to **3** (Scheme 1) is another interesting feature of anditomin biosynthesis, in which a better leaving group is generated by the acetyltransferase AndG to facilitate the following deacetation. The biosyntheses of agglomerin and quartromicin involve a similar dehydration mechanism, with the acetyltransferases Agg4 and QmnD3, respectively, but differ from the anditomin pathway in their requirement for another enzyme for the acetate elimination.[39,40] In plant isoquinoline alkaloid metabolism, salutaridinol-7-*O*-acetyltransferase catalyzes the acetylation of salutaridinol, and the resulting product then undergoes spontaneous elimination of the acetate to afford thebaine,[41] in a manner resembling the AndG-induced desaturation. However, the existence of thebaine synthase, the dedicated enzyme for deacetation and thebaine formation, was proposed.[42] Thus, the reaction by AndG represents a very rare example of enzymatic acetylation-mediated dehydration, and also suggests the existence of a similar mechanism for double bond formation in other biosynthetic pathways.

Notably, in this study, we were able to elucidate the full biosynthetic route to **1**, by characterizing the functions of all of the enzymes involved in the pathway. Targeted gene-deletion experiments are widely applied to biosynthetic studies, and are a powerful tool to predict the functions of each gene in the biosynthetic gene cluster and the biosynthetic pathway. However, the complete determination of the pathway is often hampered, due to the lack of intermediate accumulation upon gene disruption. With the heterologous expression system in *A. oryzae*, we succeeded in the unambiguous determination of the anditomin pathway, confirming the significant advantage of the heterologous expression approach in biosynthetic studies on fungal natural products.

Finally, the anditomin pathway involves several intriguing chemistries, and both AndA and AndF are catalysts for unique oxidative rearrangements in fungal secondary metabolism.[4] Especially, the synthesis of the intramolecular bridged structure by AndA is astonishing. Interestingly, the originally proposed Diels−Alder reaction inspired synthetic chemists to perform the biomimetic synthesis with the analogue of the predicted intermediate, which successfully generated the same bicyclo[2.2.2]octane system as in andilesins.[43] The reaction, however, requires high temperature (>80 °C) and a long time (5 days) and also yields an undesired regioisomer. In contrast to this Diels−Alder reaction, the radical-based reaction by AndA is much faster and moderate, and occurs with precise product selectivity. Thus, the mechanism by which AndA controls the reaction is extremely interesting, but still remains elusive. However, it is also possible that AndA is only responsible for the generation of the C-12 radical, and the rearrangement is a fortuitous gift due to the substrate structure elaborately designed by nature.

■ CONCLUSION

After over 30 years since the isolation of anditomin (**1**) in 1981, we now report the first elucidation of the molecular basis for anditomin biosynthesis. The anditomin pathway involves 12 enzymes directly, and adopts a somewhat different early stage biosynthesis from the other DMOA-derived meroterpenoid pathways for terretonin, austinol, and andrastin A. The initially proposed Diels−Alder reaction is not actually utilized by the pathway, but alternatively, the fungus employs an unprecedented synthetic strategy with the dioxygenase AndA to afford the unique bicyclo[2.2.2]octane framework. This study indicates that nature's synthetic approaches are still beyond our imagination, and many exciting chemistries remain to be discovered in natural product biosyntheses.

In conclusion, we have established the complete biosynthetic pathway of **1**, by isolating almost all of the intermediates using *A. oryzae* heterologous expression systems. We believe that this approach is a very powerful tool for the elucidation of biosynthetic pathways and the isolation of natural product precursors. As the molecular bases for several DMOA-derived meroterpenoids are now well-understood, in future studies, novel molecules with useful activities could be obtained by rationally or randomly combining the genes derived from different pathways.

■ MATERIALS AND METHODS

Strains and Media. *Emericella variecolor* NBRC 32302 was obtained from the Biological Resource Center, National Institute of Technology and Evaluation (Chiba, Japan). *E. variecolor* NBRC 32302 was cultivated at 30 °C, 160 rpm in DPY medium (2% dextrin, 1% hipolypepton (Nihon Pharmaceutical Co., Ltd.), 0.5% yeast extract (Difco), 0.5% KH_2PO_4, and 0.05% $MgSO_4{\cdot}7H_2O$) for 3 days, and used as a source for whole genome sequencing and the cloning of each gene in the *and* cluster. For the isolation of anditomin (**1**), the strain was statically cultivated at 28 °C in malt extract broth (3% malt extract (Difco), containing 0.5% mycological peptone (Oxoid)) for 10 days.

Aspergillus oryzae NSAR1 (*niaD*$^-$, *sC*$^-$, Δ*argB*, *adeA*$^-$)[29] was used as the host for fungal expression. Transformants of the *A. oryzae* strain were grown in shaking cultures in DPY medium for 6 days at 30 °C and at 160 rpm. The cells were then transferred into Czapek-Dox (CD) medium with hipolypepton (10 g/L), and starch (20 g/L) to induce expression under the α-amylase promoter, and the cultures were shaken for further three to 6 days.

Standard DNA engineering experiments were performed using *Escherichia coli* DH5α, purchased from Clontech (Mountain View, CA). *E. coli* cells carrying each plasmid were grown in Luria−Bertani medium and were selected with appropriate antibiotics. *E. coli* Rosetta2(DE3) (Novagen) was used for the expression of AndA, and *E. coli* BL21-CodonPlus(DE3)-RIL (Agilent Technologies) was used for the expression of AndF and AndG.

Whole Genome Sequencing and Analysis. Genome sequencing of *E. variecolor* NBRC 32302 was performed by Hokkaido System Science Co., Ltd. (Hokkaido, Japan) with an Illumina HiSeq 2000 system. Sequence assembly was performed with Velvet[44] version 1.2.08 (http://www.ebi.ac.uk/~zerbino/velvet/) to yield 630 contigs covering approximately 33.5 Mb. Gene prediction was then performed with AUGUSTUS[45] (http://bioinf.uni-greifswald.de/webaugustus/) and manually revised by comparisons with homologous genes found in the NCBI database, if necessary. All of the products of the predicted genes were used to construct the database for the local BLAST search.

Construction of the Fungal Expression Vector pBARI. To construct the fungal expression vector with the glufosinate-resistance gene, *bar*, the region encoding the *ptrA* gene of pPTRI vector[46] (TaKaRa) was replaced with that of *bar*. The region encoding *bar* was amplified from the pBARGPE1 vector[47] with primers bar-pPTRI-F and bar-pPTRI-R (Table S1). Linear pPTRI, lacking the region encoding *ptrA*, was amplified with the primers pPTRI-F and pPTRI-R (Table S1). The PCR products were purified and then ligated using an In-Fusion HD Cloning Kit (Clontech Laboratories, Inc.), according to the manufacturer's protocol, to yield the plasmid designated as pBARI.

Construction of Fungal Expression Plasmids. For the construction of one-gene containing fungal expression plasmids, each gene in the *and* cluster was amplified from *E. variecolor* NBRC 32302 genomic DNA, with the primers listed in Tables S1 and S2. The full-length *and* genes were purified, digested with appropriate restriction enzymes, if necessary, and ligated into the pTAex3,[48] pUSA,[49] or pUNA[50] vectors using an In-Fusion HD Cloning Kit or Ligation Kit Ver. 2.1 (TaKaRa) according to the manufacturer's protocol (Table S2). For introduction into pAdeA,[51] pPTRI, and pBARI, a fragment containing the *amyB* promoter (*PamyB*) and the *amyB* terminator (*TamyB*) was amplified from the pTAex3-based plasmids and ligated into each vector (Table S2).

To construct the coexpression plasmid of *andK* and *andD*, pTAex3-andD was digested with *Bam*HI to yield the DNA fragment containing *PamyB-andD-TamyB*. This fragment was ligated into pUSA-andK, which had been digested with *Bam*HI and dephosphorylated, to produce pTAex3-andK+D. For the other coexpression plasmids, two different gene fragments with both or either *PamyB* and *TamyB* were amplified from pTAex3-based plasmids and ligated into each vector, to generate the two-gene containing plasmids (Table S2).

Transformation of *Aspergillus oryzae* NSAR1. Transformation of *A. oryzae* NSAR1 was performed by the protoplast−polyethylene glycol method reported previously.[52] To coexpress *andM, andK, andD, andE*, and *andB*, three plasmids, pTAex3-andM, pUSA-andK+D, and pAdeA-andE+B, were used for the transformation. The resultant transformant was transformed with pUNA-andC+A and pPTRI-andJ +I to construct the nine gene-expression system, which was further transformed with pBARI-andG+H to generate the 11 gene-expressing strain. When constructing the transformants with *andA, andC, andF, andH, andI*, and *andJ*, three plasmids, pTAex3-andA+C, pUSA-andC +H, pAdeA-andI+J, were used. For the construction of negative control strains that do not express one or more genes, the corresponding void vectors or plasmids with only one gene were used for the transformation.

HPLC Analysis of Each Product. Products from each of the transformants and the in vitro reaction mixture were analyzed by HPLC, with a solvent system of 0.5% acetic acid (solvent A) and acetonitrile containing 0.5% acetic acid (solvent B), at a flow rate of 1.0 mL/min and a column temperature of 40 °C. Separation was performed with solvent B/solvent A (20:80) for 5 min, a linear gradient from 20:80 to 100:0 within the following 20 min, 100:0 for 5 additional min, and a linear gradient from 100:0 to 20:80 within the following 3 min.

Isolation and Purification of Each Metabolite. For the isolation of each metabolite, media from one liter of the culture were extracted with ethyl acetate. Mycelia were extracted with acetone at room temperature overnight, concentrated, and reextracted with ethyl acetate. Both extracts were combined and subjected to silica-gel column chromatography and further purification by preparative HPLC. The detailed purification procedures for each compound are described in the Supporting Information.

Expression and Purification of AndA, AndF, and AndG. To express *andA*, *andF*, and *andG* in *E. coli*, each gene was introduced into the pET-28a(+) vector (Novagen). The full-length *and* genes were amplified with the primers listed in Tables S1 and S2, purified, digested with *Nde*I and *Eco*RI, and ligated into the pET-28a(+) vector using a Ligation Kit Ver. 2.1 (Table S2).

For the expression of AndA, *E. coli* Rosetta2(DE3) was transformed with the pET-28a(+)-andA plasmid. The transformant was incubated with shaking at 37 °C/160 rpm, in LB medium supplemented with 50 mg/L kanamycin sulfate. Gene expression was induced by the addition of 0.5 mM IPTG when the cultures had grown to an OD_{600} of 0.6, after which the incubation was continued for 15 h at 20 °C/160 rpm. The cells were harvested by centrifugation, resuspended in lysis buffer (50 mM Tris, pH 7.5, 150 mM NaCl, 5 mM imidazole, 5% glycerol), and lysed on ice by sonication. The cell debris was removed by centrifugation, and the supernatant was loaded onto a Ni-NTA affinity column, which was washed with 30 column volumes of wash buffer (50 mM Tris, pH 7.5, 150 mM NaCl, 10 mM imidazole, 5% glycerol). The his-tagged protein was eluted with 5 column volumes of elution buffer (50 mM Tris, pH 7.5, 150 mM NaCl, 300 mM imidazole, 5% glycerol). The purity of the enzymes was analyzed by sodium dodecyl sulfate polyacrylamide gel electrophoresis (SDS-PAGE). The protein concentration was determined using a UV-1700 PharmaSpec Spectrophotometer (Shimadzu).

To express AndF or AndG, *E. coli* BL21-CodonPlus(DE3)-RIL was transformed with pET-28a(+)-andF or pET-28a(+)-andG, respectively. Each transformant was incubated with shaking at 37 °C/160 rpm, in LB medium supplemented with 50 mg/L kanamycin sulfate. Gene expression was induced by the addition of 0.5 mM IPTG when the cultures had grown to an OD_{600} of 0.6, after which the incubation was continued for 20 h at 18 °C/160 rpm. The purification procedures were the same as those mentioned above for AndA.

Enzymatic Reaction Assay of AndA. The enzymatic reaction of AndA with preandiloid B (**10**) and preandiloid C (**11**) was performed in reaction mixtures containing 50 mM Tris-HCl buffer (pH 7.5), 500 μM of **10** or **11**, 0.1 mM $FeSO_4$, 2.5 mM α-ketoglutarate, 4 mM ascorbate, and 5.8 μM AndA, in a final volume of 50 μL. After an incubation at 30 °C for 3 h, the reaction was terminated by adding 50 μL of methanol and mixed by vortex. After centrifugation, the supernatant was analyzed by HPLC and LC−MS/MS.

Enzymatic Reaction Assay of AndG. The enzymatic reaction of AndG with andilesin A (**2**) was performed in a reaction mixture containing 50 mM Tris-HCl buffer (pH 7.5), 500 μM of **2**, 2 mM acetyl coenzyme A, and 8.6 μM AndG, in a final volume of 50 μL. After an incubation at 30 °C for 3 h, the reaction was terminated by adding 50 μL of methanol and mixed by vortex. After centrifugation, the supernatant was analyzed by HPLC and LC−MS/MS.

Acetylation of Andilesin A (2). Acetic anhydride (128.0 mg) was added to a solution of **2** (1.79 mg) in dry pyridine (300 μL) at 65 °C. After 8 h, the reaction mixture was diluted with methanol and analyzed by HPLC and LC−MS/MS.

Enzymatic Reaction Assay of AndF. The enzymatic reaction of AndF with andilesin C (**4**) was performed in a reaction mixture containing 50 mM Tris-HCl buffer (pH 8.0), 500 μM of **4**, 0.1 mM $FeSO_4$, 2.5 mM α-ketoglutarate, 4 mM ascorbate, and 7.4 μM AndF, in a final volume of 50 μL. After an incubation at 30 °C for 3 h, the reaction was terminated by adding 50 μL of methanol and mixed by vortex. After centrifugation, the supernatant was analyzed by HPLC and LC−MS/MS.

*3,5-Dimethylorsellinic Acid (DMOA, **5**).* Yellowish white solid; for UV spectrum see Figure S1; for ^1H and ^{13}C NMR data see Table S3; HRMS found m/z 179.0711 $[M - H_2O + H]^+$ (calcd 179.0708 for $C_{10}H_{11}O_3$). The NMR data are in good agreement with the reported data.[20]

*5,7-Dihydroxy-4,6-dimethylphthalide (DHDMP, **6**).* Yellowish white solid; for UV spectrum see Figure S1; for ^1H and ^{13}C NMR data see Table S4; HRMS found m/z 195.0655 $[M + H]^+$ (calcd

195.0657 for $C_{10}H_{11}O_4$). The NMR data are in good agreement with the reported data.[53]

Farnesyl-DHDMP (7). Yellowish oil; $[\alpha]^{20}_D$ −37.7 (*c* 1.00, $CHCl_3$) ; for UV spectrum see Figure S1; for ^1H and ^{13}C NMR data see Table S5 and Figures S10 and S11; HRMS found *m*/*z* 421.2339 $[M + Na]^+$ (calcd 421.2355 for $C_{25}H_{34}O_4Na$).

Dihydroxyfarnesyl-DHDMP (8′). Yellowish oil; $[\alpha]^{20}_D$ −87.1 (*c* 1.00, $CHCl_3$); for UV spectrum see Figure S1; for ^1H and ^{13}C NMR data see Table S6 and Figures S12 and S13; HRMS found *m*/*z* 455.2403 $[M + Na]^+$ (calcd 455.2410 for $C_{25}H_{36}O_6Na$).

Preandiloid A (9). White amorphous solid; $[\alpha]^{20}_D$ −104.8 (*c* 1.00, $CHCl_3$); for UV spectrum see Figure S1; for ^1H and ^{13}C NMR data see Table S7 and Figure S14 and S15; HRMS found *m*/*z* 415.2485 $[M + H]^+$ (calcd 415.2485 for $C_{25}H_{35}O_5$).

Preandiloid B (10). White amorphous solid; $[\alpha]^{20}_D$ −33.9 (*c* 1.00, $CHCl_3$); for UV spectrum see Figure S1; for ^1H and ^{13}C NMR data see Table S8 and Figures S16 and S17; HRMS found *m*/*z* 413.2317 $[M + H]^+$ (calcd 413.2328 for $C_{25}H_{33}O_5$).

Preandiloid C (11). White amorphous solid; $[\alpha]^{20}_D$ −53.9 (*c* 0.53, $CHCl_3$); for UV spectrum see Figure S1; for ^1H and ^{13}C NMR data see Table S9 and Figures S18 and S19; HRMS found *m*/*z* 411.2164 $[M + H]^+$ (calcd 411.2172 for $C_{25}H_{31}O_5$).

Andiconin (12). Colorless needles; $[\alpha]^{20}_D$ −80.7 (*c* 1.00, $CHCl_3$); for UV spectrum see Figure S1; for ^1H and ^{13}C NMR data see Table S10 and Figures S20 and S21; HRMS found *m*/*z* 411.2158 $[M + H]^+$ (calcd 411.2172 for $C_{25}H_{31}O_5$).

Andilesin D (13). White amorphous solid; $[\alpha]^{20}_D$ −87.0 (*c* 0.46, acetone); for UV spectrum see Figure S1; for ^1H and ^{13}C NMR data see Table S11 and Figures S22 and S23; HRMS found *m*/*z* 427.2120 $[M + H]^+$ (calcd 427.2121 for $C_{25}H_{31}O_6$).

Andilesin A (2). Colorless needles; $[\alpha]^{20}_D$ −4.8 (*c* 1.00, $CHCl_3$); for UV spectrum see Figure S1; for ^1H and ^{13}C NMR data see Table S12 and Figures S24 and S25; HRMS found *m*/*z* 429.2289 $[M + H]^+$ (calcd 429.2277 for $C_{25}H_{33}O_6$). The NMR data are in good agreement with the reported data,[9] but are slightly revised and updated in this study.

Andilesin B (3). White solid; $[\alpha]^{20}_D$ −257.2 (*c* 0.59, $CHCl_3$); for UV spectrum see Figure S1; for ^1H and ^{13}C NMR data see Table S13 and Figures S26 and S27; HRMS found *m*/*z* 411.2155 $[M + H]^+$ (calcd 411.2172 for $C_{25}H_{31}O_5$). The NMR data are in good agreement with the reported data,[9] but are slightly revised and updated in this study.

Andilesin C (4). Colorless needles; $[\alpha]^{20}_D$ −0.8 (*c* 0.61, $CHCl_3$); for UV spectrum see Figure S1; for ^1H and ^{13}C NMR data see Table S14 and Figures S28 and S29; HRMS found *m*/*z* 413.2332 $[M + H]^+$ (calcd 413.2328 for $C_{25}H_{33}O_5$). The NMR data are in good agreement with the reported data,[9] but are slightly revised and updated in this study.

Anditomin (1). White solid; $[\alpha]^{20}_D$ +68.8 (*c* 0.16, $CHCl_3$); for UV spectrum see Figure S1; for ^1H and ^{13}C NMR data see Table S15 and Figures S30 and S31; HRMS found *m*/*z* 411.2192 $[M + H]^+$ (calcd 411.2172 for $C_{25}H_{31}O_5$). The NMR data are in good agreement with the reported data,[10,13] but are slightly revised and updated in this study.

■ ASSOCIATED CONTENT

Ⓢ Supporting Information

Experimental details, supplementary figures, and spectral data are provided. This material is available free of charge via the Internet at http://pubs.acs.org. Sequence data for the *and* cluster have been deposited at DDBJ/EMBL/GenBank under accession AB981314.

■ AUTHOR INFORMATION

Corresponding Author

abei@mol.f.u-tokyo.ac.jp

Notes

The authors declare no competing financial interest.

■ ACKNOWLEDGMENTS

We thank Prof. K. Gomi (Tohoku University) and Prof. K. Kitamoto (The University of Tokyo) for kindly providing the expression vectors and the fungal strain. This work was supported by Grants-in-Aid for Scientific Research from the Ministry of Education, Culture, Sports, Science and Technology, Japan.

■ REFERENCES

(1) Fischbach, M. A.; Walsh, C. T. *Chem. Rev.* **2006**, *106*, 3468−3496.
(2) Hur, G. H.; Vickery, C. R.; Burkart, M. D. *Nat. Prod. Rep.* **2012**, *29*, 1074−1098.
(3) Gao, Y.; Honzatko, R. B.; Peters, R. J. *Nat. Prod. Rep.* **2012**, *29*, 1153−1175.
(4) Cox, R. J. *Nat. Prod. Rep.* **2014**, *31*, 1405−1424.
(5) Hu, Y.; Dietrich, D.; Xu, W.; Patel, A.; Thuss, J. A.; Wang, J.; Yin, W.-B.; Qiao, K.; Houk, K.; Vederas, J. C. *Nat. Chem. Biol.* **2014**, *10*, 552−554.
(6) Chooi, Y.-H.; Hong, Y. J.; Cacho, R. A.; Tantillo, D. J.; Tang, Y. *J. Am. Chem. Soc.* **2013**, *135*, 16805−16808.
(7) Dunn, A. W.; Johnstone, R. A.; Sklarz, B.; King, T. J. *J. Chem. Soc., Chem. Commun.* **1976**, 270−270.
(8) Dunn, A. W.; Johnstone, R. A. W.; Sklarz, B.; Lessinger, L.; King, T. J. *J. Chem. Soc., Chem. Commun.* **1978**, 533−534.
(9) Simpson, T. J. *J. Chem. Soc., Perkin Trans. 1* **1979**, 2118−2121.
(10) Simpson, T. J.; Walkinshaw, M. D. *J. Chem. Soc., Chem. Commun.* **1981**, 914−915.
(11) Liangsakul, J.; Pornpakakul, S.; Sangvichien, E.; Muangsin, N.; Sihanonth, P. *Tetrahedron Lett.* **2011**, *52*, 6427−6430.
(12) Holker, J. S. E.; Simpson, T. J. *J. Chem. Soc., Chem. Commun.* **1978**, 626−627.
(13) Simpson, T. J. *Tetrahedron Lett.* **1981**, *22*, 3785−3788.
(14) Bartlett, A. J.; Holker, J. S.; O'Brien, E.; Simpson, T. J. *J. Chem. Soc., Chem. Commun.* **1981**, 1198−1200.
(15) McIntyre, C. R.; Scott, F. E.; Simpson, T. J.; Trimble, L. A.; Vederas, J. C. *J. Chem. Soc., Chem. Commun.* **1986**, 501−503.
(16) Simpson, T. J.; Ahmed, S. A.; McIntyre, C. R.; Scott, F. E.; Sadler, I. H. *Tetrahedron* **1997**, *53*, 4013−4034.
(17) Kim, H. J.; Ruszczycky, M. W.; Liu, H.-w. *Curr. Opin. Chem. Biol.* **2012**, *16*, 124−131.
(18) Geris, R.; Simpson, T. J. *Nat. Prod. Rep.* **2009**, *26*, 1063−1094.
(19) Lo, H.-C.; Entwistle, R.; Guo, C.-J.; Ahuja, M.; Szewczyk, E.; Hung, J.-H.; Chiang, Y.-M.; Oakley, B.; Wang, C. C. *J. Am. Chem. Soc.* **2012**, *134*, 4709−4720.
(20) Itoh, T.; Tokunaga, K.; Radhakrishnan, E. K.; Fujii, I.; Abe, I.; Ebizuka, Y.; Kushiro, T. *ChemBioChem* **2012**, *13*, 1132−1135.
(21) Matsuda, Y.; Awakawa, T.; Itoh, T.; Wakimoto, T.; Kushiro, T.; Fujii, I.; Ebizuka, Y.; Abe, I. *ChemBioChem* **2012**, *13*, 1738−1741.
(22) Guo, C.-J.; Knox, B. P.; Chiang, Y.-M.; Lo, H.-C.; Sanchez, J. F.; Lee, K.-H.; Oakley, B. R.; Bruno, K. S.; Wang, C. C. *Org. Lett.* **2012**, *14*, 5684−5687.
(23) Matsuda, Y.; Awakawa, T.; Abe, I. *Tetrahedron* **2013**, *69*, 8199−8204.
(24) Matsuda, Y.; Awakawa, T.; Wakimoto, T.; Abe, I. *J. Am. Chem. Soc.* **2013**, *135*, 10962−10965.
(25) Nielsen, M. L.; Nielsen, J. B.; Rank, C.; Klejnstrup, M. L.; Holm, D. K.; Brogaard, K. H.; Hansen, B. G.; Frisvad, J. C.; Larsen, T. O.; Mortensen, U. H. *FEMS Microbiol. Lett.* **2011**, *321*, 157−166.
(26) Regueira, T. B.; Kildegaard, K. R.; Hansen, B. G.; Mortensen, U. H.; Hertweck, C.; Nielsen, J. *Appl. Environ. Microbiol.* **2011**, *77*, 3035−3043.
(27) Hansen, B. G.; Mnich, E.; Nielsen, K. F.; Nielsen, J. B.; Nielsen, M. T.; Mortensen, U. H.; Larsen, T. O.; Patil, K. R. *Appl. Environ. Microbiol.* **2012**, *78*, 4908−4913.
(28) al Fahad, A.; Abood, A.; Simpson, T. J.; Cox, R. J. *Angew. Chem.* **2014**, *126*, 7649−7653.

(29) Jin, F. J.; Maruyama, J.; Juvvadi, P. R.; Arioka, M.; Kitamoto, K. *FEMS Microbiol. Lett.* **2004**, *239*, 79−85.
(30) Tagami, K.; Liu, C.; Minami, A.; Noike, M.; Isaka, T.; Fueki, S.; Shichijo, Y.; Toshima, H.; Gomi, K.; Dairi, T. *J. Am. Chem. Soc.* **2013**, *135*, 1260−1263.
(31) Sakai, K.; Kinoshita, H.; Nihira, T. *Appl. Microbiol. Biotechnol.* **2012**, *93*, 2011−2022.
(32) Guo, C.-J.; Knox, B.; Chiang, Y.-M.; Lo, H.-C.; Sanchez, J.; Lee, K.-H.; Oakley, B.; Bruno, K.; Wang, C. C. *Org. Lett.* **2012**, *14*, 5684−5687.
(33) Steffan, N.; Grundmann, A.; Afiyatullov, S.; Ruan, H.; Li, S.-M. *Org. Biomol. Chem.* **2009**, *7*, 4082−4087.
(34) Kato, N.; Suzuki, H.; Takagi, H.; Uramoto, M.; Takahashi, S.; Osada, H. *ChemBioChem* **2011**, *12*, 711−714.
(35) Nicholson, M. J.; Koulman, A.; Monahan, B. J.; Pritchard, B. L.; Payne, G. A.; Scott, B. *Appl. Environ. Microbiol.* **2009**, *75*, 7469−7481.
(36) Cueto, M.; MacMillan, J. B.; Jensen, P. R.; Fenical, W. *Phytochemistry* **2006**, *67*, 1826−1831.
(37) Kovaleva, E. G.; Lipscomb, J. D. *Nat. Chem. Biol.* **2008**, *4*, 186−193.
(38) Cohen, E.; Koch, L.; Thu, K. M.; Rahamim, Y.; Aluma, Y.; Ilan, M.; Yarden, O.; Carmeli, S. *Biorg. Med. Chem.* **2011**, *19*, 6587−6593.
(39) Kanchanabanca, C.; Tao, W.; Hong, H.; Liu, Y.; Hahn, F.; Samborskyy, M.; Deng, Z.; Sun, Y.; Leadlay, P. F. *Angew. Chem.* **2013**, *125*, 5897−5900.
(40) Wu, L.-F.; He, H.-Y.; Pan, H.-X.; Han, L.; Wang, R.; Tang, G.-L. *Org. Lett.* **2014**, *16*, 1578−1581.
(41) Grothe, T.; Lenz, R.; Kutchan, T. M. *J. Biol. Chem.* **2001**, *276*, 30717−30723.
(42) Fisinger, U.; Grobe, N.; Zenk, M. H. *Nat. Prod. Commun.* **2007**, *2*, 249−253.
(43) Spangler, J. E.; Sorensen, E. J. *Tetrahedron* **2009**, *65*, 6739−6745.
(44) Zerbino, D. R.; Birney, E. *Genome Res.* **2008**, *18*, 821−829.
(45) Stanke, M.; Schöffmann, O.; Morgenstern, B.; Waack, S. *BMC Bioinf.* **2006**, *7*, 62.
(46) Kubodera, T.; Yamashita, N.; Nishimura, A. *Biosci. Biotechnol. Biochem.* **2000**, *64*, 1416−1421.
(47) Pall, M. L.; Brunelli, J. *Fungal Genet. Newsl.* **1993**, *40*, 59−62.
(48) Fujii, T.; Yamaoka, H.; Gomi, K.; Kitamoto, K.; Kumagai, C. *Biosci. Biotechnol. Biochem.* **1995**, *59*, 1869−1874.
(49) Yamada, O.; Na Nan, S.; Akao, T.; Tominaga, M.; Watanabe, H.; Satoh, T.; Enei, H.; Akita, O. *J. Biosci. Bioeng.* **2003**, *95*, 82−88.
(50) Yamada, O.; Lee, B. R.; Gomi, K.; Iimura, Y. *J. Biosci. Bioeng.* **1999**, *87*, 424−429.
(51) Jin, F.; Maruyama, J.; Juvvadi, P.; Arioka, M.; Kitamoto, K. *Biosci. Biotechnol. Biochem.* **2004**, *68*, 656−662.
(52) Gomi, K.; Iimura, Y.; Hara, S. *Agric. Biol. Chem.* **1987**, *51*, 2549−2555.
(53) Tsunematsu, Y.; Ichinoseki, S.; Nakazawa, T.; Ishikawa, N.; Noguchi, H.; Hotta, K.; Watanabe, K. *J. Antibiot.* **2012**, *65*, 377−380.